JHEP

Published for SISSA by Springer

Received: April 28, 2021
Revised: July 14, 2021
Accepted: July 15, 2021
Published: August 4, 2021

JHEP08(2021)021

$A_{\rm FB}$ in the SMEFT: precision Z physics at the LHC

Víctor Bresó-Pla,[a] **Adam Falkowski**[b] **and Martín González-Alonso**[a]

[a] *Departament de Física Teòrica, IFIC, Universitat de València - CSIC, Apt. Correus 22085, E-46071 València, Spain*

[b] *CNRS/IN2P3, IJCLab, Université Paris-Saclay, 91405 Orsay, France*

E-mail: vicbreso@ific.uv.es, adam.falkowski@cern.ch, martin.gonzalez@ific.uv.es

Abstract: We study the forward-backward asymmetry $A_{\rm FB}$ in $pp \to \ell^+\ell^-$ at the Z peak within the Standard Model Effective Field Theory (SMEFT). We find that this observable provides per mille level constraints on the vertex corrections of the Z boson to quarks, which close a flat direction in the electroweak precision SMEFT fit. Moreover, we show that current $A_{\rm FB}$ data is precise enough so that its inclusion in the fit improves significantly LEP bounds even in simple New Physics setups. This demonstrates that the LHC can compete with and complement LEP when it comes to precision measurements of the Z boson properties.

Keywords: Beyond Standard Model, Effective Field Theories

ArXiv ePrint: 2103.12074

https://doi.org/10.1007/JHEP08(2021)021

Contents

1 Introduction

Precision measurements represent a crucial ingredient in the search of physics beyond the Standard Model (SM). It is of the utmost importance to analyze such measurements within general frameworks to minimize the theoretical bias. The Standard Model Effective Field Theory (SMEFT) [1, 2] is greatly suited for that purpose, since its only assumption is the existence of a large gap between the electroweak scale and the masses of particles beyond the SM. The SMEFT represents a robust theoretical approach that is systematically improvable, that benefits from the well-known Effective Field Theory (EFT) machinery and that can be applied to a plethora of New Physics models [3]. Its application to study the effect of heavy new particles in precision measurements is particularly convenient since these measurements are typically carried out at relatively low energies (at or below the electroweak scale).

The electroweak sector is one of the cornerstones of the SM, with all interactions fixed by the gauge symmetries, with the only free parameters being the gauge couplings. At the end of the previous century, experiments in the LEP collider confirmed the robustness of the SM gauge structure to a remarkable precision. Arguably, the most important legacy of LEP is a set of electroweak precision measurements of the masses and partial decay widths of the Z and W bosons [4, 5]. The precision program initiated by LEP has exerted enormous influence on the particle physics research. On one hand, it offered historically important

JHEP08(2021)021

guidelines for subsequent discoveries of the remaining SM degrees of freedom: the top quark and the Higgs boson. On the other hand, it severely restricted the options for new physics near the electroweak scale. In this latter context, the benefits of model-independent characterization of electroweak precision observables were quickly recognized, first in the framework of the oblique parameters [6], and later in the general EFT framework [7].

The Tevatron and the LHC also have a place in this endeavour. First, they allow us to expand the precision program onto the top and the Higgs sectors. But even in the field of the classic electroweak observables hadron colliders have a chance to compete, despite having a less clean environment than LEP. This was spectacularly demonstrated by the ATLAS measurement of the W mass [8], which now dominates the global average [9]. Also the total width [10, 11] and certain ratios of leptonic decay widths [12–14] of the W boson are measured more precisely in hadron colliders than in LEP-2. A similar result is however lacking regarding the Z boson mass and couplings. Naively, this is understandable, as in this case hadron colliders have to compete with a per mille or better accuracy of LEP-1. For instance, the determinations of the weak mixing angle at the LHC [15–17] are currently at least a factor of three less precise than the one in LEP.

In this paper we provide a proof-of-principle demonstration that the LHC precision measurements at the Z-pole can compete with and complement LEP. This is the case when electroweak precision measurements are interpreted within the SMEFT framework. As we will show, LEP alone cannot simultaneously constrain all higher-dimensional SMEFT operators that modify the Z boson coupling to the up and down quarks. Hadron colliders, which probe exactly these couplings when (in particular) the colliding quarks annihilate into an on-shell Z-boson, can deliver the missing pieces of information.

Our study will rest on Drell-Yan dilepton production, $pp \to \ell^+\ell^-$. The LHC collaborations have published precise measurements of the differential cross-sections in this process [13, 15–19]. In fact, this is the same process from which the LHC determinations of the SM weak mixing angle are extracted, which, as mentioned above, cannot yet compete with LEP. But the comparison between LEP and LHC is altered once contributions from physics beyond the SM are considered. The fact that LHC measurements of the differential cross-section in $pp \to \ell^+\ell^-$ agree with the SM predictions to such a high precision represents a nontrivial constraint on possible non-standard contributions. The same holds for different extractions of the weak angle, which are in general sensitive to different New Physics effects. However, the extraction of such bounds cannot be carried out from the results of the SM analysis, but requires a dedicated study.

In the context of the SMEFT, it is known that the study of $pp \to \ell^+\ell^-$ events with high invariant dilepton masses provides strong constraints on 4-fermion contact interactions [20–22]. This is so because the latter grow with the energy of the process, contrary to the SM contribution, which is suppressed at high energies by the Z propagator. However, the situation is quite different for the couplings of the Z boson to fermions (Zff). Measurements carried out by LEP1 at the Z peak were able to probe these couplings with very high accuracy. Contrary to the case of 4-fermion interactions, the contributions to the $pp \to Z/\gamma^* \to l^+l^-$ cross-section from non-standard Zff couplings do not grow with energy. Thus one might naively expect that LHC data will not improve significantly our knowledge of the Zff couplings.

JHEP08(2021)021

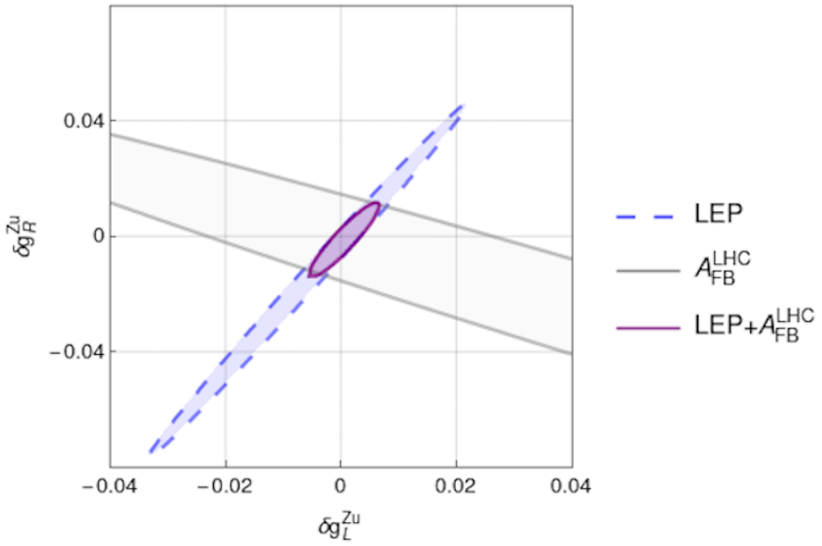

Figure 1. Allowed regions (at 95% CL) for the corrections of the Z couplings to left- and right-handed up quarks. All other couplings are assumed to be given by their SM values. The marginalized bounds at 95% CL are $\delta g_L^{Zu} \in [-0.028, 0.017], \delta g_R^{Zu} \in [-0.064, 0.035]$ for the "LEP" fit and $\delta g_L^{Zu} \in [-0.004, 0.005], \delta g_R^{Zu} \in [-0.012, 0.009]$ for the "LEP+$A_{\rm FB}^{\rm LHC}$" fit.

The purpose of this work is to study qualitatively and quantitatively this question in the SMEFT setup. In order to do that, we focus on the forward-backward (FB) asymmetry, $A_{\rm FB}$, which is particularly clean both experimentally and theoretically [18, 19, 23, 24]. Contrary to the naive expectation, we find that current $A_{\rm FB}$ measurements provide unique information about the Z couplings to quarks that improve significantly LEP-only bounds. This is true not just in complicated scenarios requiring intricate cancellations between many Wilson Coefficients, but also in simple theory setups. To illustrate this last point, we anticipate one of our results in figure 1, which shows the experimental bounds on possible modifications of the Z couplings to left- and right-handed up quarks, assuming all other interactions are SM-like. The impact of the inclusion of LHC $A_{\rm FB}$ data is clear. The reason why LHC can improve on the LEP determination of the Zuu couplings is that the latter suffers from large correlations.

The rest of this work is organized as follows. In section 2 we describe the SMEFT theory setup, and in section 3 we review the constraints obtained from "traditional" pole data (mainly LEP, but not only). Section 4 represents the main element of this work. The $pp \to \ell^+\ell^-$ FB asymmetry is introduced and used to extract bounds on the Zqq vertex corrections, which are then compared with LEP bounds. Finally, section 5 contains our conclusions.

2 Theory framework

The SMEFT Lagrangian [1, 2] is organized into an expansion in $1/\Lambda^2$, where Λ is interpreted as the mass scale of new particles in the UV completion of this EFT. We truncate the expansion at $\mathcal{O}(\Lambda^{-2})$, that is, we neglect operators with dimensions higher than six. The

JHEP08(2021)021

Lagrangian takes the form

$$\mathcal{L}_{\rm SMEFT} = \mathcal{L}_{\rm SM} + \frac{1}{\Lambda^2}\sum_i c_i\, O_i^{D=6}, \tag{2.1}$$

where $\mathcal{L}_{\rm SM}$ is the SM Lagrangian, each $O_i^{D=6}$ is a gauge-invariant operator of dimension D=6, and c_i are the corresponding Wilson coefficients. $O_i^{D=6}$ span the complete space of dimension-6 operators, see refs. [25, 26] for examples of such sets.

The SMEFT Lagrangian contains all fundamental interactions predicted in the SM, as well as new interactions and deformations of the SM ones due to the dimension-6 operators. In this paper we focus on Z and W pole observables, which are mainly sensitive to non-derivative interactions between the heavy electroweak vector bosons and fermions. We parametrize them as

$$\begin{aligned}
\mathcal{L}_{\rm SMEFT} \supset & -\frac{g_L}{\sqrt{2}}\left(W_\mu^+ \bar{u}_L \gamma_\mu (V + \delta g_L^{Wq}) d_L + W_\mu^+ \bar{u}_R \gamma_\mu \delta g_R^{Wq} d_R + \text{h.c.}\right) \\
& - \frac{g_L}{\sqrt{2}}\left(W_\mu^+ \bar{\nu}_L \gamma_\mu (\mathbf{I} + \delta g_L^{We}) e_L + \text{h.c.}\right) \\
& - \sqrt{g_L^2 + g_Y^2} Z_\mu \left[\sum_{f\in u,d,e,\nu} \bar{f}_L \gamma_\mu ((T_f^3 - s_\theta^2 Q_f)\,\mathbf{I} + \delta g_L^{Zf}) f_L\right] \\
& - \sqrt{g_L^2 + g_Y^2} Z_\mu \left[\sum_{f\in u,d,e} \bar{f}_R \gamma_\mu (-s_\theta^2 Q_f\,\mathbf{I} + \delta g_R^{Zf}) f_R\right].
\end{aligned} \tag{2.2}$$

In this Lagrangian, the SM fermion fields f are 3-vectors in the flavor space, written in the basis where their mass terms are diagonal (for neutrinos, where their charged current interactions are diagonal in the limit $\delta g_L^{We} \to 0$), $s_\theta^2 = g_Y^2/(g_Y^2 + g_L^2)$ is the sine squared of the weak mixing angle and V is the unitary CKM matrix. The SM massive vector fields are denoted as $W_\mu^\pm$ and Z_μ. In our conventions, their mass terms take the form

$$\mathcal{L}_{\rm SMEFT} \supset \frac{g_L^2 v^2}{4}(1+\delta m_w)^2 W_\mu^+ W_\mu^- + \frac{(g_L^2+g_Y^2)v^2}{8} Z_\mu Z_\mu. \tag{2.3}$$

Here, g_L, g_Y are the electroweak couplings, and v is the Higgs VEV. These electroweak parameters are assigned numerical values by matching them to the input observables G_F, $\alpha(m_Z)$, m_Z:

$$g_L = 0.6485, \quad g_Y = 0.3580, \quad v = 246.22\ \text{GeV}, \tag{2.4}$$

where the errors can be ignored for the present purpose. The input observables are expressed in terms of the electroweak parameters as $G_F = (\sqrt{2}v^2)^{-1}$, $\alpha(m_Z) = g_L^2 g_Y^2/(4\pi(g_L^2+g_Y^2))$, $m_Z = \sqrt{g_L^2+g_Y^2}\,v/2$, i.e. all the corrections due to the dimension-6 operators and loops are absorbed in the definition of g_L, g_Y, v. Given the numerical values in eq. (2.4), the strength of the non-derivative $Vf\bar{f}$ interactions is completely fixed in the SM in terms of the fermions' quantum numbers: the weak isospin T_f^3, and the electric charge Q_f. As shown in eq. (2.2), deformations of these interactions due to the dimension-6 operators are parametrized by the *vertex corrections* δg, which are 3×3 matrices in the flavor space and can be flavor-violating. They can be expressed as linear combinations of

JHEP08(2021)021

the Wilson coefficients c_i in eq. (2.1) and they are $\mathcal{O}(\Lambda^{-2})$ in the EFT counting. Not all the δg's are independent in the SMEFT framework where dimension-8 and higher operators are neglected. Expressing δg by the Wilson coefficients in any basis one finds the relation

$$\delta g_L^{Z\nu} = \delta g_L^{We} + \delta g_L^{Ze}, \qquad \delta g_L^{Wq} = \delta g_L^{Zu} V - V \delta g_L^{Zd} \,. \tag{2.5}$$

In this work we restrict our attention to the flavor-diagonal part of δg. We also approximate V by the unit matrix when it acts on $\mathcal{O}(\Lambda^{-2})$ terms.[1]

The focus of this paper is the new physics effects parametrized by the diagonal elements of δg in eq. (2.2). On the experimental side we restrict ourselves to the so-called *pole observables*, where a single Z or W boson is produced and decays on-shell. The important feature of this class of observables is that, at leading order, new physics enters *only* via δg. Other effects of dimension-6 operators enter the pole observables with various suppression factors. In particular, the contributions from 4-fermion operators are suppressed by $\Gamma_V/m_V \sim 1/16\pi^2$ [7] or by a loop factor [28] relatively to those of δg and are neglected here. As for the dipole interactions, $d_f \bar{f} \sigma_{\mu\nu} f V_{\mu\nu}$, their interference with the SM amplitudes is suppressed by the small fermion masses, while the quadratic effects in d_i are $\mathcal{O}(\Lambda^{-4})$ in the EFT expansion and are consistently neglected. Thus, restricting to pole observables largely simplifies the analysis, allowing one to avoid dealing with the huge parameter space of the SMEFT and instead to focus on a relatively small number of parameters δg. To be specific, we will discuss model-independent constraints on the following 20 independent real parameters:

$$\delta g_L^{We}, \, \delta g_L^{W\mu}, \, \delta g_L^{W\tau}, \, \delta g_{L/R}^{Ze}, \, \delta g_{L/R}^{Z\mu}, \, \delta g_{L/R}^{Z\tau}, \, \delta g_{L/R}^{Zd}, \, \delta g_{L/R}^{Zs}, \, \delta g_{L/R}^{Zb}, \, \delta g_{L/R}^{Zu}, \, \delta g_{L/R}^{Zc}, \, \delta m_w. \tag{2.6}$$

As mentioned earlier, in this paper we do not consider observables targeting flavor-off-diagonal elements of the δg matrices. Therefore all δg's above refer to the diagonal elements, for which we will employ the shorter notation: $\delta g_X^{Vf_J} \equiv [\delta g_X^{Vf}]_{JJ}$. We also do not consider top observables, therefore we do not provide constraints on $\delta g_{L/R}^{Zt}$. As for δg_R^{Wq}, they affect the pole observables quadratically (because there are no SM right-handed currents to interfere with) and thus are neglected as $\mathcal{O}(\Lambda^{-4})$ effects. Finally, $\delta g_L^{Z\nu}$ and δg_L^{Wq} can be expressed by the vertex corrections in eq. (2.6) by virtue of eq. (2.5).

We will present our results in the form of a likelihood function for the parameters in eq. (2.6), which encodes simultaneous constraints on the 19 δg's and δm_w including all correlations. This can be translated into constraints on the Wilson coefficients in the reader's favorite basis, provided the map between δg and the Wilson coefficients is known.[2] In appendix A we provide the map relating δg to the Wilson coefficients of the commonly used Warsaw basis [25].

[1] Going beyond this approximation requires introducing some input scheme for the CKM matrix elements [27].

[2] Alternatively, one can use the Higgs basis defined in ref. [29], where δg's play the role of the Wilson coefficients and no translation is needed.

JHEP08(2021)021

3 Traditional pole observables

The traditional Z-pole observables are those carried out at LEP-1 and SLC, which we list in table 1. The experimental values are taken from the classic report of ref. [4], with minor modifications affecting the Z width, the hadronic cross section σ_{had} and the FB asymmetry of b quarks to take into account the recent results of refs. [30, 31]. We also include the measurements of A_s and R_{uc} [9, 32] that, despite being less precise, are needed to remove flat directions in the EFT parameter space.

In the case of the W boson, the traditional pole observables were carried out at LEP-2, Tevatron and LHC, and they are summarized in table 2. We stress that this dataset includes recent LHC results concerning the leptonic branching ratios of the W boson [12, 14, 33]. Once again, we include the not-so-precise measurements of R_{Wc} [9] to remove flat directions.

We use these pole observables to constrain the EFT coefficients in eq. (2.6). For that we build the associated χ^2 function

$$\chi^2 = \sum_{ij} \left[O_{i,\text{exp}} - O_{i,\text{th}}\right] (\sigma^{-2})_{ij} \left[O_{j,\text{exp}} - O_{j,\text{th}}\right], \tag{3.1}$$

where σ^{-2} is the inverse of the covariance matrix, and the theory prediction of each observable is given by

$$O_{i,\text{th}} = O_{i,\text{SM}} + \sum_k \alpha_{ik}\, \delta g_k\,, \tag{3.2}$$

where δg_k runs over all the couplings listed in eq. (2.6). For the SM predictions of the Z observables in table 1 we use the values obtained in ref. [35], which are calculated using the couplings in eq. (2.4) and the known state-of-the-art expressions. For the W observables in table 2 we use the SM predictions from ref. [36], except for the W mass where we use the semi-analytic expression from ref. [37]. The uncertainties of the SM predictions are subleading compared to the experimental uncertainties and will be neglected in this work. In our analysis we use the α_{ik} coefficients in eq. (3.2) calculated at tree-level. Log-enhanced one-loop corrections generated through running to higher/lower scales can be included via the renormalization group equation [38]. Finite loop corrections [28] are neglected in this work; see e.g. [39] for estimates of their effects in the context of a different fit. We minimize the χ^2 function with all δg corrections and δm_w present simultaneously. Although all the 20 coefficients are kept all the time (and their bounds are correlated), it is instructive to discuss the results by groups. For the leptonic couplings, we find the following central values and 1σ errors:

$$[\delta g_L^{We}]_{ii} = \begin{pmatrix} -1.3 \pm 3.2 \\ -2.8 \pm 2.6 \\ 1.5 \pm 4.0 \end{pmatrix} \times 10^{-3}, \tag{3.3}$$

$$[\delta g_L^{Ze}]_{ii} = \begin{pmatrix} -0.19 \pm 0.28 \\ 0.1 \pm 1.2 \\ -0.09 \pm 0.59 \end{pmatrix} \times 10^{-3}, \quad [\delta g_R^{Ze}]_{ii} = \begin{pmatrix} -0.43 \pm 0.27 \\ 0.0 \pm 1.4 \\ 0.62 \pm 0.62 \end{pmatrix} \times 10^{-3}\,. \tag{3.4}$$

JHEP08(2021)021

Observable	*Experimental value*	*SM prediction*	*Definition*
Γ_Z [GeV]	2.4955 ± 0.0023 [4, 30]	2.4941	$\sum_f \Gamma(Z \to f\bar{f})$
σ_{had} [nb]	41.4802 ± 0.0325 [4, 30]	41.4842	$\frac{12\pi}{m_Z^2}\frac{\Gamma(Z\to e^+e^-)\Gamma(Z\to q\bar{q})}{\Gamma_Z^2}$
R_e	20.804 ± 0.050 [4]	20.734	$\frac{\sum_q \Gamma(Z\to q\bar{q})}{\Gamma(Z\to e^+e^-)}$
R_μ	20.785 ± 0.033 [4]	20.734	$\frac{\sum_q \Gamma(Z\to q\bar{q})}{\Gamma(Z\to \mu^+\mu^-)}$
R_τ	20.764 ± 0.045 [4]	20.781	$\frac{\sum_q \Gamma(Z\to q\bar{q})}{\Gamma(Z\to \tau^+\tau^-)}$
$A_{\text{FB}}^{0,e}$	0.0145 ± 0.0025 [4]	0.0162	$\frac{3}{4}A_e^2$
$A_{\text{FB}}^{0,\mu}$	0.0169 ± 0.0013 [4]	0.0162	$\frac{3}{4}A_eA_\mu$
$A_{\text{FB}}^{0,\tau}$	0.0188 ± 0.0017 [4]	0.0162	$\frac{3}{4}A_eA_\tau$
R_b	0.21629 ± 0.00066 [4]	0.21581	$\frac{\Gamma(Z\to b\bar{b})}{\sum_q \Gamma(Z\to q\bar{q})}$
R_c	0.1721 ± 0.0030 [4]	0.1722	$\frac{\Gamma(Z\to c\bar{c})}{\sum_q \Gamma(Z\to q\bar{q})}$
A_b^{FB}	0.0996 ± 0.0016 [4, 31]	0.1032	$\frac{3}{4}A_eA_b$
A_c^{FB}	0.0707 ± 0.0035 [4]	0.0736	$\frac{3}{4}A_eA_c$
A_e	0.1516 ± 0.0021 [4]	0.1470	$\frac{\Gamma(Z\to e_L^+e_L^-)-\Gamma(Z\to e_R^+e_R^-)}{\Gamma(Z\to e^+e^-)}$
A_μ	0.142 ± 0.015 [4]	0.1470	$\frac{\Gamma(Z\to \mu_L^+\mu_L^-)-\Gamma(Z\to \mu_R^+\mu_R^-)}{\Gamma(Z\to \mu^+\mu^-)}$
A_τ	0.136 ± 0.015 [4]	0.1470	$\frac{\Gamma(Z\to \tau_L^+\tau_L^-)-\Gamma(Z\to \tau_R^+\tau_R^-)}{\Gamma(Z\to \tau^+\tau^-)}$
A_e	0.1498 ± 0.0049 [4]	0.1470	$\frac{\Gamma(Z\to e_L^+e_L^-)-\Gamma(Z\to e_R^+e_R^-)}{\Gamma(Z\to e^+e^-)}$
A_τ	0.1439 ± 0.0043 [4]	0.1470	$\frac{\Gamma(Z\to \tau_L^+\tau_L^-)-\Gamma(Z\to \tau_R^+\tau_R^-)}{\Gamma(Z\to \tau^+\tau^-)}$
A_b	0.923 ± 0.020 [4]	0.935	$\frac{\Gamma(Z\to b_L\bar{b}_L)-\Gamma(Z\to b_R\bar{b}_R)}{\Gamma(Z\to b\bar{b})}$
A_c	0.670 ± 0.027 [4]	0.668	$\frac{\Gamma(Z\to c_L\bar{c}_L)-\Gamma(Z\to c_R\bar{c}_R)}{\Gamma(Z\to c\bar{c})}$
A_s	0.895 ± 0.091 [32]	0.936	$\frac{\Gamma(Z\to s_L\bar{s}_L)-\Gamma(Z\to s_R\bar{s}_R)}{\Gamma(Z\to s\bar{s})}$
R_{uc}	0.166 ± 0.009 [9]	0.172	$\frac{\Gamma(Z\to u\bar{u})+\Gamma(Z\to c\bar{c})}{2\sum_q \Gamma(Z\to q\bar{q})}$

Table 1. *Z pole observables.* The experimental errors of the observables not separated by horizontal lines are correlated, which is taken into account in the fit. The first A_e and A_τ values come from the combination of leptonic polarization and left-right asymmetry measurements at SLD, while the second values come from the LEP-1 measurements of the polarization of the $\tau^\pm$ leptons.

JHEP08(2021)021

Observable	*Experimental value*	*SM prediction*
m_W [GeV]	80.379 ± 0.012 [9]	80.356
Γ_W [GeV]	2.085 ± 0.042 [9]	2.088
$\mathrm{Br}(W \to e\nu)$	0.1071 ± 0.0016 [5]	0.1082
$\mathrm{Br}(W \to \mu\nu)$	0.1063 ± 0.0015 [5]	0.1082
$\mathrm{Br}(W \to \tau\nu)$	0.1138 ± 0.0021 [5]	0.1081
$\mathrm{Br}(W \to \mu\nu)/\mathrm{Br}(W \to e\nu)$	0.982 ± 0.024 [34]	1.000
$\mathrm{Br}(W \to \mu\nu)/\mathrm{Br}(W \to e\nu)$	1.020 ± 0.019 [12]	1.000
$\mathrm{Br}(W \to \mu\nu)/\mathrm{Br}(W \to e\nu)$	1.003 ± 0.010 [13]	1.000
$\mathrm{Br}(W \to \tau\nu)/\mathrm{Br}(W \to e\nu)$	0.961 ± 0.061 [9, 33]	0.999
$\mathrm{Br}(W \to \tau\nu)/\mathrm{Br}(W \to \mu\nu)$	0.992 ± 0.013 [14]	0.999
$R_{Wc} \equiv \frac{\Gamma(W\to cs)}{\Gamma(W\to ud)+\Gamma(W\to cs)}$	0.49 ± 0.04 [9]	0.50

Table 2. *W pole observables.* The experimental errors of the observables not separated by horizontal lines are correlated, which is taken into account in the fit.

For the couplings involving strange, charm and bottom quarks, we obtain

$$\delta g_L^{Zs} = (1.3 \pm 4.1) \times 10^{-2}, \qquad \delta g_R^{Zs} = (2.2 \pm 5.6) \times 10^{-2}, \tag{3.5}$$

$$\delta g_L^{Zc} = (-1.3 \pm 3.7) \times 10^{-3}, \qquad \delta g_R^{Zc} = (-3.2 \pm 5.4) \times 10^{-3}, \tag{3.6}$$

$$\delta g_L^{Zb} = (3.1 \pm 1.7) \times 10^{-3}, \qquad \delta g_R^{Zb} = (21.8 \pm 8.8) \times 10^{-3}\,. \tag{3.7}$$

The data also constrain the SMEFT corrections to the W mass: $\delta m_w = (2.9 \pm 1.6) \times 10^{-4}$. We see that the Z and W pole observables in tables 1 and 2 simultaneously constrain all leptonic and heavy quark vertex corrections with (typically) per mille level accuracy. On the other hand, they *cannot* simultaneously constrain all light quark vertex corrections; in fact, only 3 linear combinations of δg_L^{Zu}, δg_R^{Zu}, δg_L^{Zd} and δg_R^{Zd} are probed by these observables. It is possible to show that the linear combination

$$\delta g_L^{Zu} + \delta g_L^{Zd} + \frac{3g_L^2 - g_Y^2}{4g_Y^2}\delta g_R^{Zu} + \frac{3g_L^2 + g_Y^2}{2g_Y^2}\delta g_R^{Zd} \tag{3.8}$$

is *not* probed at all by the observables in tables 1 and 2. In other words, it is a flat direction in the $\mathcal{O}(\Lambda^{-2})$ EFT fit. In order to characterize the constraints on the light quark couplings, it is convenient to introduce new variables x, y, z, t related by a rotation to the light quark vertex corrections:

$$\begin{pmatrix} x \\ y \\ z \\ t \end{pmatrix} = R \begin{pmatrix} \delta g_L^{Zu} \\ \delta g_R^{Zu} \\ \delta g_L^{Zd} \\ \delta g_R^{Zd} \end{pmatrix} = \begin{pmatrix} 0.93 & -0.29 & -0.23 & -0.01 \\ 0.18 & 0.87 & -0.33 & -0.33 \\ 0.27 & 0.18 & 0.90 & -0.29 \\ 0.17 & 0.37 & 0.17 & 0.90 \end{pmatrix} \begin{pmatrix} \delta g_L^{Zu} \\ \delta g_R^{Zu} \\ \delta g_L^{Zd} \\ \delta g_R^{Zd} \end{pmatrix}, \tag{3.9}$$

JHEP08(2021)021

where R is an SO(4) matrix such that: 1) t is proportional to the flat direction in eq. (3.8); 2) x, y, z are mutually uncorrelated in the fit. The combinations x, y, z are constrained by the above-discussed pole observables with percent-level accuracy:

$$\begin{pmatrix} x \\ y \\ z \end{pmatrix} = \begin{pmatrix} -0.9 \pm 1.8 \\ 0.3 \pm 3.3 \\ -2.4 \pm 4.8 \end{pmatrix} \times 10^{-2}. \tag{3.10}$$

As defined above, the fourth combination t is not constrained by the observables in tables 1 and 2. Another experimental input is needed to lift the flat direction, and thus to simultaneously constrain all four light quark vertex corrections. In ref. [40] the measurement of $Zq\bar{q}$ couplings in Tevatron's D0 [41] is employed to that purpose. However the resulting limit is very loose: $t = (0.1 \pm 17) \times 10^{-2}$, which is an order of magnitude weaker than the constraints in eq. (3.10) on the remaining three combinations.

In the following of this paper we show that leptonic Z asymmetries at the LHC provide a more promising and more precise route to constrain t and lift the flat direction in the SMEFT fit of W and Z pole observables.

4 Hadron colliders as probes of Zqq couplings

The presence of the flat direction given in eq. (3.8) and the precise LHC/Tevatron extractions of the weak angle suggest that measurements of on-shell Z production in hadron colliders can be important from the global SMEFT perspective, even if the accuracy is somewhat inferior compared to the most precise LEP-1 measurements. The goal of this section is to study this in detail.

4.1 The Drell-Yan forward-backward asymmetry at the LHC

The natural LHC process to probe the Z interactions with light quarks is the Drell-Yan production of lepton pairs, $pp \to Z/\gamma^* \to l^+l^-$. Indeed, at the parton level the intermediate Z is produced via $q\bar{q} \to Z$, providing tree-level sensitivity to the Zqq couplings. We will focus on the FB asymmetry in the Drell-Yan production, which is a particularly clean observable thanks to cancellations of various QCD and PDF uncertainties, and for which high precision has been achieved both on the experimental and the theory side [18, 19, 23, 24]. This observable has been used to extract with high accuracy the weak mixing angle [17], and it is currently being discussed as a possible tool to further constrain the parton distribution functions [42, 43].

At the partonic level, the asymmetry appears in the decay angle θ^* of the negatively charged lepton with respect to the incoming quark direction in the center of mass frame. It is non-zero already in the SM, due to parity-violating Z couplings to fermions. In the SM the differential cross section of the partonic process $q\bar{q} \to Z/\gamma^* \to \ell^+\ell^-$ is given at leading order by [44]:

$$\begin{aligned} \frac{d\hat{\sigma}_{q\bar{q}}\left(\hat{s}, cos\theta^*\right)}{d\cos\theta^*} &\propto \hat{\sigma}^{\text{even}}_{q\bar{q}}\left(\hat{s}, \cos\theta^*\right) + \hat{\sigma}^{\text{odd}}_{q\bar{q}}\left(\hat{s}, \cos\theta^*\right) \\ &\propto H^{\text{even}}_{q\bar{q}}\left(\hat{s}\right)\left(1 + \cos^2\theta^*\right) + H^{\text{odd}}_{q\bar{q}}\left(\hat{s}\right)\cos\theta^*, \end{aligned} \tag{4.1}$$

JHEP08(2021)021

where

$$H_{q\bar{q}}^{\text{even}}(\hat{s}) = \frac{3}{2}\frac{\hat{s}}{\left(\hat{s}-m_Z^2\right)^2+m_Z^2\Gamma_Z^2}\left(\left(g_V^{Zq}\right)^2+\left(g_A^{Zq}\right)^2\right)\left(\left(g_V^{Zl}\right)^2+\left(g_A^{Zl}\right)^2\right)+$$
$$+\frac{3\left(Q_q\right)^2\left(Q_l\right)^2}{2\hat{s}}+\frac{3\left(\hat{s}-m_Z^2\right)}{\left(\hat{s}-m_Z^2\right)^2+m_Z^2\Gamma_Z^2}Q_qQ_l\,g_V^{Zq}g_V^{Zl}, \tag{4.2}$$

$$H_{q\bar{q}}^{\text{odd}}(\hat{s}) = \frac{12\hat{s}}{\left(\hat{s}-m_Z^2\right)^2+m_Z^2\Gamma_Z^2}g_V^{Zq}g_A^{Zq}g_V^{Zl}g_A^{Zl}+\frac{6\left(\hat{s}-m_Z^2\right)}{\left(\hat{s}-m_Z^2\right)^2+m_Z^2\Gamma_Z^2}Q_qQ_l\,g_A^{Zq}g_A^{Zl}. \tag{4.3}$$

Here, $\hat{s}$ is the invariant mass of the dilepton system, Q_f are the electric charges and $g_{V/A}^{Zf} \equiv g_R^{Zf} \pm g_L^{Zf}$ are the vector/axial couplings of the Z boson to fermions. It is trivial to include the effect of SMEFT corrections to the Zff couplings in the differential cross-sections given above. As long as we stay near the Z pole ($\hat{s} \approx M_Z$) the corrections due to 4-fermion SMEFT operators are suppressed by $\Gamma_Z/m_Z \sim 0.02$, and can be neglected in the leading order approximation.[3] Note that there are no vertex corrections to photon couplings.

The term proportional to $\cos\theta^*$ in eq. (4.1) will induce a difference in the number of events with a negative lepton going in the forward ($\cos\theta^* > 0$) and backward ($\cos\theta^* < 0$) directions. This asymmetry cannot be directly observed at the LHC because there we are not dealing with quarks as incoming particles, but with protons. Thus, we must modify eq. (4.1) by including parton distribution functions (PDFs). Moreover, having two identical particles in the initial state introduces an important complication: the absence of a preferred direction that one can use to build an asymmetry. In other words, we do not know *in every individual event* which proton contains the quark and which one contains the antiquark that are annihilating. In order to circumvent this issue, the asymmetry is defined with respect to the longitudinal boost of the dilepton system on an event-by-event basis. Equivalently, one assumes that the momentum of the quark is larger than that of the antiquark [23, 24, 44], which is only true on average. This inevitably introduces a distorsion on the asymmetry at the parton level, which can be analytically parametrized through a dilution factor, as shown below.

An additional complication arises because (anti)quarks might have non-zero transverse momentum, which impedes us from equating the direction of the quark-antiquark pair in the partonic interaction to the beam direction. This effect can be minimized working in the so-called Collins-Soper frame [45], where θ^* is defined as the angle between ℓ^- and the axis that bisects the angle between the quark-momentum direction and the opposite directions to the antiquark momentum. This subtlety is not relevant for our work, which is restricted to studying the tree-level SMEFT corrections, in which case the transverse momentum of the incoming quarks is zero.

All in all, once these changes are implemented, eq. (4.1) transforms into [44]:

$$\frac{d\sigma_{pp}(Y,\hat{s},\cos\theta^*)}{dY\,d\hat{s}\,d\cos\theta^*} \propto \sum_{q=u,d,s,c,b}\left[\hat{\sigma}_{q\bar{q}}^{\text{even}}(\hat{s},\cos\theta^*)+D_{q\bar{q}}(Y,\hat{s})\,\hat{\sigma}_{q\bar{q}}^{\text{odd}}(\hat{s},\cos\theta^*)\right]F_{q\bar{q}}(Y,\hat{s}), \tag{4.4}$$

[3] Note that finite (i.e. not log-enhanced) 1-loop SMEFT corrections, also neglected in our approximation, are suppressed by a numerically similar factor.

JHEP08(2021)021

where Y is the rapidity of the dilepton center-of-mass system, $F_{q\bar{q}}(Y,\hat{s})$ is called the parton factor and $D_{q\bar{q}}(Y,\hat{s})$ is the dilution factor to which we alluded previously. They depend on the PDFs as:

$$F_{q\bar{q}}(Y,\hat{s}) = f_q\left(e^{+Y}\sqrt{\frac{\hat{s}}{s}},\hat{s}\right) f_{\bar{q}}\left(e^{-Y}\sqrt{\frac{\hat{s}}{s}},\hat{s}\right) + f_q\left(e^{-Y}\sqrt{\frac{\hat{s}}{s}},\hat{s}\right) f_{\bar{q}}\left(e^{+Y}\sqrt{\frac{\hat{s}}{s}},\hat{s}\right), \quad (4.5)$$

$$D_{q\bar{q}}(Y,\hat{s}) = \frac{f_q\left(e^{+|Y|}\sqrt{\frac{\hat{s}}{s}},\hat{s}\right) f_{\bar{q}}\left(e^{-|Y|}\sqrt{\frac{\hat{s}}{s}},\hat{s}\right) - f_q\left(e^{-|Y|}\sqrt{\frac{\hat{s}}{s}},\hat{s}\right) f_{\bar{q}}\left(e^{+|Y|}\sqrt{\frac{\hat{s}}{s}},\hat{s}\right)}{F_{q\bar{q}}(\hat{s},Y)}, \quad (4.6)$$

where s is the proton-proton invariant mass. Using this hadronic differential cross-section, the FB asymmetry is defined as:

$$A_{\rm FB}(Y,\hat{s}) = \frac{\sigma_F(Y,\hat{s}) - \sigma_B(Y,\hat{s})}{\sigma_F(Y,\hat{s}) + \sigma_B(Y,\hat{s})}, \quad (4.7)$$

where the forward and backward cross-sections, σ_F and σ_B, are obtained by integrating the differential cross section over the positive and negative values of $\cos\theta^*$, respectively. It should also be noted that, to calculate $A_{\rm FB}$ integrated over the Y and $\hat{s}$ bins, one should integrate independently σ_F and σ_B and then calculate the integrated $A_{\rm FB}$ from that input.[4]

The dependence of the asymmetry on the invariant mass and rapidity of the dilepton system effectively increase the number of independent observables at our disposal. In this work we restrict to the dilepton masses close to the Z peak, so that contributions from 4-fermion operators can be neglected and only vertex corrections need to be considered. Corrections to the leptonic Z couplings can also be neglected, due to the very stringent LEP-1 constraints shown in eq. (3.4). The effects due to the vertex correction involving the s, b and c are suppressed by the small PDFs of the heavy quarks in the proton, and again can be neglected given the LEP-1 constraints. Using measurements of the asymmetry at different rapidity bins, we will be able to probe different combinations of Zqq couplings. In principle, four distinct rapidity bins are enough to disentangle all four $\delta g_{L/R}^{Zd/Zu}$ corrections, although this may be hindered in practice by large correlations between the bins, as we will see in the following.

4.2 Numerical analysis

In this section we set bounds on the Z couplings to light quarks using the measurement of the ATLAS collaboration of the angular distributions of leptons from the Drell-Yan process in the $\sqrt{s} = 8\,\text{TeV}$ data [46]. In particular we will use the measurement of the so-called A_4 angular coefficient, which is defined upon expanding the Drell-Yan differential cross section in harmonic polynomials, and it is related to the FB asymmetry by $A_{\rm FB} = (3/8)A_4$. This

[4] We have checked that the width of the $\hat{s}$-bin (20 GeV) is small enough so that 4-fermion operators can be safely neglected in our analysis. More precisely, the contributions proportional to 4-fermion Wilson coefficients C_{4F} (measured in units of $1/v^2$) are suppressed by numerical factors of order 0.01. Given the constraints from high-p_T tails of the Drell-Yan distributions at the LHC, which typically require $|C_{4F}| < 10^{-3}$ [22], the 4-fermion contribution at the Z-pole are completely unobservable with the current accuracy.

JHEP08(2021)021

|Y|	*Experimental value*	*SM prediction*
0.0 – 0.8	0.0195 ± 0.0015	0.0144 ± 0.0007
0.8 – 1.6	0.0448 ± 0.0016	0.0471 ± 0.0017
1.6 – 2.5	0.0923 ± 0.0026	0.0928 ± 0.0021
2.5 – 3.6	0.1445 ± 0.0046	0.1464 ± 0.0021

Table 3. ATLAS A_4 measurements obtained in ref. [46] using $\sqrt{s} = 8\,\text{TeV}$ data for a dilepton invariant mass in the range $(80\,\text{GeV}, 100\,\text{GeV})$. The SM predictions, obtained at NNLO in QCD, are also taken from ref. [46].

equation holds at all orders in QCD when considering the full phase space of the individual decay leptons. Thus, the results of the previous sections are immediately applicable to this measurement, up to the trivial 3/8 numerical factor.

Table 3 shows the results of the ATLAS measurements of A_4 for dileptons at the Z peak ($80\,\text{GeV} < \sqrt{\hat{s}} < 100\,\text{GeV}$). As we can see, the asymmetry was measured for four values of the dilepton rapidity, which will allow us to separate (at least formally) the four corrections of the Z boson to up and down quarks. Table 3 also shows the SM predictions, as given in the ATLAS paper [46], which were calculated at NNLO in QCD [47–49].[5] We can see that, contrary to the electroweak observables discussed in section 3, the theory errors are comparable to the experimental ones and cannot be neglected.

The theory predictions are modified in the presence of nonstandard corrections. Working at linear order in them we have:

$$A_{4,i}^{\text{th}} = A_{4,i}^{\text{SM}} \left(1 + \alpha_{ik}\, \delta g_k\right) \tag{4.8}$$

where the i index corresponds to the four rapidity bins (see table 3) and $\delta g_k = \{g_L^{Zu}, g_R^{Zu}, g_L^{Zd}, g_R^{Zd}\}$. The numerical factors α_{ik} are calculated using eqs. (4.4)–(4.7), after integration over the $\hat{s}$ and Y bins and using the MMHT2014lo68cl PDF set [50]. The uncertainties of this PDF set and those obtained changing the PDF set were calculated but, since their impact on our final results is negligible, we will ignore them hereafter.

We use this semi-analytical approach, instead of a purely numerical one, because the cross section we are interested in is free of kinematic cuts, except for those on the dilepton invariant mass and rapidity. This follows from the definition of the A_4 angular coefficient, which includes an integration over the whole individual lepton phase space, which is carried out experimentally through an unfolding procedure [46]. Our semi-analytical approach simplifies the analysis and avoids uncertainties from the numerical simulation, which may be significant due to the small size of the FB asymmetry. Nonetheless, we have crosschecked our results using a numerical approach, in which the cross sections are calculated using MadGraph [51] and processed by MadAnalysis5 [52]. Neglected contributions from parton shower or detector effects are expected to be small for this process, which only involves light leptons in the final state.

[5] Similar Drell-Yan studies by CMS [17, 18] and LHCb [15] do not provide explicitly the SM predictions for their observables and often do not probe the dependence on the dilepton rapidity. We also limit ourselves to $\sqrt{s} = 8\,\text{TeV}$ data because currently there are no A_{FB} measurements at higher energies.

JHEP08(2021)021

With the results in table 3 and eq. (4.8) we build the following χ^2 function:

$$\chi^2\left(\delta g_k\right) = \sum_i \left(\frac{A_{4,i}^{\rm SM}\left(1+\alpha_{ik}\delta g_k\right) - A_{4,i}^{\rm exp}}{\delta A_{4,i}} \right)^2 , \tag{4.9}$$

where the sum runs over the four bins of rapidity displayed in table 3. Experimental and SM errors are combined in quadrature in $\delta A_{4,i}$.

Before minimizing the full χ^2 function, it is instructive to see how each rapidity bin of the A_4 measurement performs in restricting the EFT couplings. We find:

$$\begin{aligned}
0.0 < |Y| < 0.8: &\;\; 0.63\,\delta g_L^{Zu} + 0.71\,\delta g_R^{Zu} - 0.20\,\delta g_L^{Zd} - 0.22\,\delta g_R^{Zd} = 0.088(29)\,, \\
0.8 < |Y| < 1.6: &\;\; 0.60\,\delta g_L^{Zu} + 0.74\,\delta g_R^{Zu} - 0.18\,\delta g_L^{Zd} - 0.22\,\delta g_R^{Zd} = -0.012(12)\,, \\
1.6 < |Y| < 2.5: &\;\; 0.53\,\delta g_L^{Zu} + 0.80\,\delta g_R^{Zu} - 0.16\,\delta g_L^{Zd} - 0.23\,\delta g_R^{Zd} = -0.0014(92)\,, \\
2.5 < |Y| < 3.6: &\;\; 0.43\,\delta g_L^{Zu} + 0.86\,\delta g_R^{Zu} - 0.18\,\delta g_L^{Zd} - 0.21\,\delta g_R^{Zd} = -0.0030(81)\,,
\end{aligned} \tag{4.10}$$

where we have normalized each combination to ease the comparison. We can see that the limits reach a percent-level accuracy. The limits from the lowest rapidity bin are the weakest because it is affected the most by the smearing out of the asymmetry: in this bin the direction of the boost of the dilepton system is often opposite to the direction of the incoming quark.

Let us now minimize the full likelihood in eq. (4.9), i.e., we combine the four constraints in eq. (4.10). We can see by eye that each bin constrains a similar linear combination of the quark couplings. Therefore we can already anticipate that attempts to constrain simultaneously all four vertex corrections using just the ATLAS data will suffer from large correlations. Instead, it is more instructive to show the constraints on the four linear combinations that are orthonormal and uncorrelated, which we denote as $\{x', y', z', t'\}$, similarly to our approach in section 3. We find:

$$\begin{pmatrix}
x' = 0.21\delta g_L^{Zu} + 0.19\delta g_R^{Zu} + 0.46\delta g_L^{Zd} + 0.84\delta g_R^{Zd} \\
y' = 0.03\delta g_L^{Zu} - 0.07\delta g_R^{Zu} - 0.87\delta g_L^{Zd} + 0.49\delta g_R^{Zd} \\
z' = 0.83\delta g_L^{Zu} - 0.54\delta g_R^{Zu} + 0.02\delta g_L^{Zd} - 0.10\delta g_R^{Zd} \\
t' = 0.51\delta g_L^{Zu} + 0.82\delta g_R^{Zu} - 0.17\delta g_L^{Zd} - 0.22\delta g_R^{Zd}
\end{pmatrix} = \begin{pmatrix}
-10 \pm 4 \\
0.5 \pm 0.4 \\
0.04 \pm 0.06 \\
-0.001 \pm 0.005
\end{pmatrix} . \tag{4.11}$$

As anticipated, only a single direction, which we denote as t', is constrained at 0.5% level. The constraints on the directions orthogonal to t' are much weaker, and those on x' are practically void within the EFT validity regime. This means that the ATLAS data alone cannot give us useful constraints on all Z boson couplings to quarks. Nevertheless, the input from ATLAS will be invaluable once combined with the other probes of the Zqq couplings, as we will quantify in the next subsection.

JHEP08(2021)021

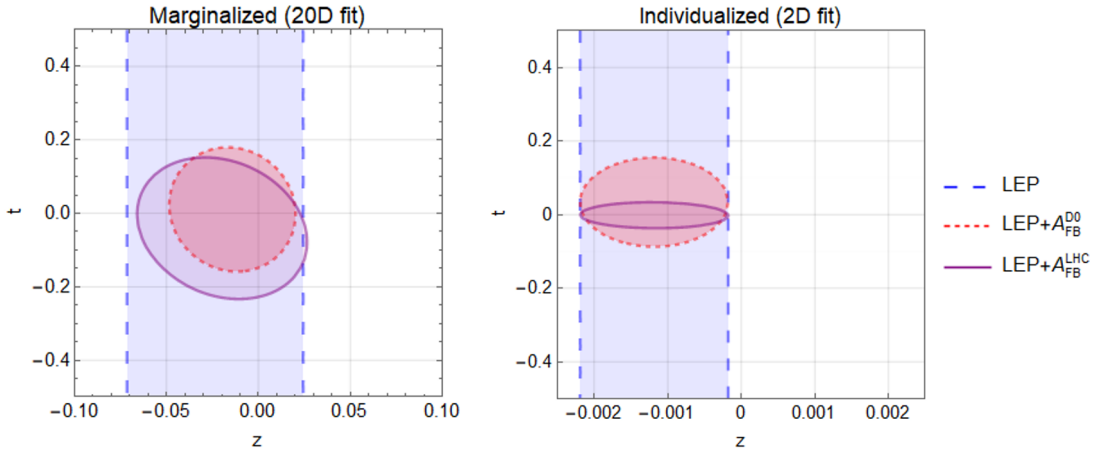

Figure 2. Allowed regions (corresponding to $\Delta\chi^2 = 1$) for the z and t combinations of vertex corrections, see eqs. (3.9) for their definition. The blue vertical band is obtained using LEP data and the rest of traditional pole observables discussed in section 3, whereas the purple and orange ellipses add the FB asymmetry measurements at LHC and D0 respectively (see main text for details). The left panel is obtained marginalizing over the remaining EFT parameters, cf. eq. (2.6), whereas the right panel is obtained setting all of them to zero. Note the horizontal scale is not the same in both plots.

4.3 Impact of A_4 on the global fit

Combining the $A_{\rm FB}$ limits obtained above with those extracted in section 3 from traditional pole data we find:

$$\begin{pmatrix} x \\ y \\ z \\ t \end{pmatrix} = \begin{pmatrix} -0.004 \pm 0.017 \\ 0.010 \pm 0.032 \\ -0.021 \pm 0.046 \\ -0.03 \pm 0.19 \end{pmatrix}, \quad \rho = \begin{pmatrix} 1. & -0.09 & -0.08 & -0.04 \\ -0.09 & 1. & -0.09 & -0.93 \\ -0.08 & -0.09 & 1. & -0.19 \\ -0.04 & -0.93 & -0.19 & 1. \end{pmatrix}. \tag{4.12}$$

Comparing with eq. (3.10), we see that the marginalized bounds on x, y and z are essentially the same, but the t combination is not anymore unconstrained. The per mille level $A_{\rm FB}$ constraint on t', cf. eq. (4.11), generates a much weaker bound on t because these combinations of Z couplings happen to be quite orthogonal ($t \cdot t' = 0.16$). In spite of this, the $A_{\rm FB}$ bound on t is stringent enough to make a significant impact when added to the traditional pole data. In eq. (4.12) this is reflected by the large correlation between y and t, which was zero before the inclusion of the $A_{\rm FB}$ data. This is illustrated in figure 2, which shows the impact of the inclusion of the FB asymmetry on the z and t combinations of vertex corrections.

Beyond the numerical impact on the extracted bounds, the inclusion of the FB asymmetry in the analysis strengthens the robustness of the EFT approach. In fact, the inclusion of $(\delta g)^2$ corrections in the analysis would have a major impact on both LEP and LHC results since $\mathcal{O}(1)$ corrections cannot be excluded by each dataset separately. However, such large corrections are not anymore possible once both datasets are used together. This is clearly illustrated in figure 3.

JHEP08(2021)021

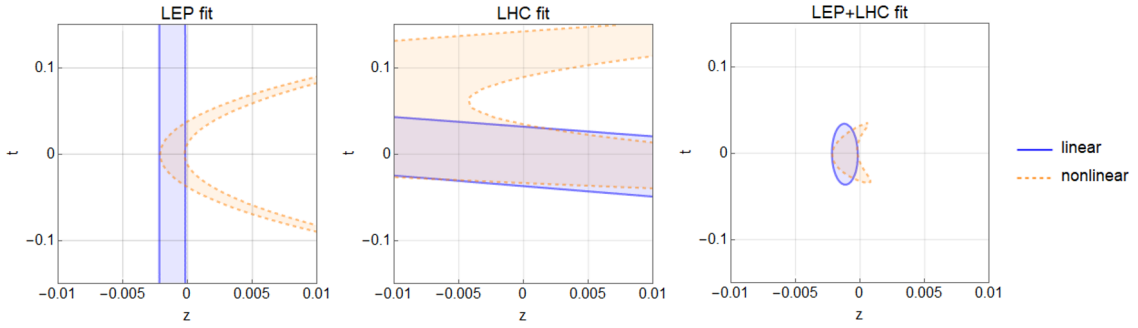

Figure 3. Comparison between linear and nonlinear contours ($\Delta\chi^2 = 1$) in a 2D fit using the "traditional" pole observables discussed in section 3 (LEP fit, left panel), the ATLAS FB asymmetry data (LHC fit, central panel) and the combination of both (right panel).

The importance of $A_{\rm FB}$ data is even clearer in simple New Physics scenarios where only some Zqq couplings are modified. This was anticipated in section 1 through figure 1, which shows the constraints on the modifications of the Z couplings to up quarks (δg_L^{Zu} and δg_R^{Zu}) assuming all other nonstandard contributions can be neglected. Figure 4 shows that the situation is similar for other pairs of vertex corrections. The fact that $A_{\rm FB}^{\rm LHC}$ provides crucial information in such simple scenarios despite the extremely precise LEP measurements is highly nontrivial and represents one of our main findings. Similar conclusions are obtained in a global SMEFT fit with specific flavor symmetries, such as $\mathrm{U}(3)^5$ and $\mathrm{U}(1)^5 \times \mathrm{U}(2)^5$.

4.4 D0 measurement

As mentioned in section 3, ref. [40] included in their dataset the determination of the light quark couplings to the Z boson at D0 [41]. This allowed them to lift the flat direction that appears when only "traditional" pole observables are used. Such determination of the light quark couplings was obtained by D0 from the FB asymmetry in $p\bar{p} \to e^+e^-$ with $5\,\mathrm{fb}^{-1}$ at $\sqrt{s} = 1.96\,\mathrm{TeV}$ [41]. That extraction used dilepton masses up to 1 TeV, so technically speaking it assumes that 4-fermion operators are absent or much smaller than vertex corrections. However, one expects that the D0 determination is dominated by the bins near the Z-pole, which have the largest statistics. This is confirmed by our simulations. For this reason, the removal of off-peak bins is not expected to change the D0 extraction of the vertex corrections.

Such D0 results are sensitive to individual vertex corrections at the 2%-level or worse, which is ~ 4 times weaker than the sensitivity of the LHC $A_{\rm FB}$ data, cf. eq. (4.11). Combining the traditional observables from section 3 with the D0 input we obtain:

$$\begin{pmatrix} x \\ y \\ z \\ t \end{pmatrix} = \begin{pmatrix} -0.009 \pm 0.017 \\ 0.007 \pm 0.023 \\ -0.014 \pm 0.034 \\ 0.01 \pm 0.17 \end{pmatrix}, \quad \rho = \begin{pmatrix} 1 & -0.19 & 0.18 & 0.00 \\ -0.19 & 1 & 0.04 & -0.68 \\ 0.18 & 0.04 & 1 & -0.07 \\ 0.00 & -0.68 & -0.07 & 1 \end{pmatrix}. \tag{4.13}$$

The comparison of the D0 limits with the LHC+LEP results of eq. (4.12) is complicated because one has to compare marginalized bounds *and* correlations. The former are more

JHEP08(2021)021

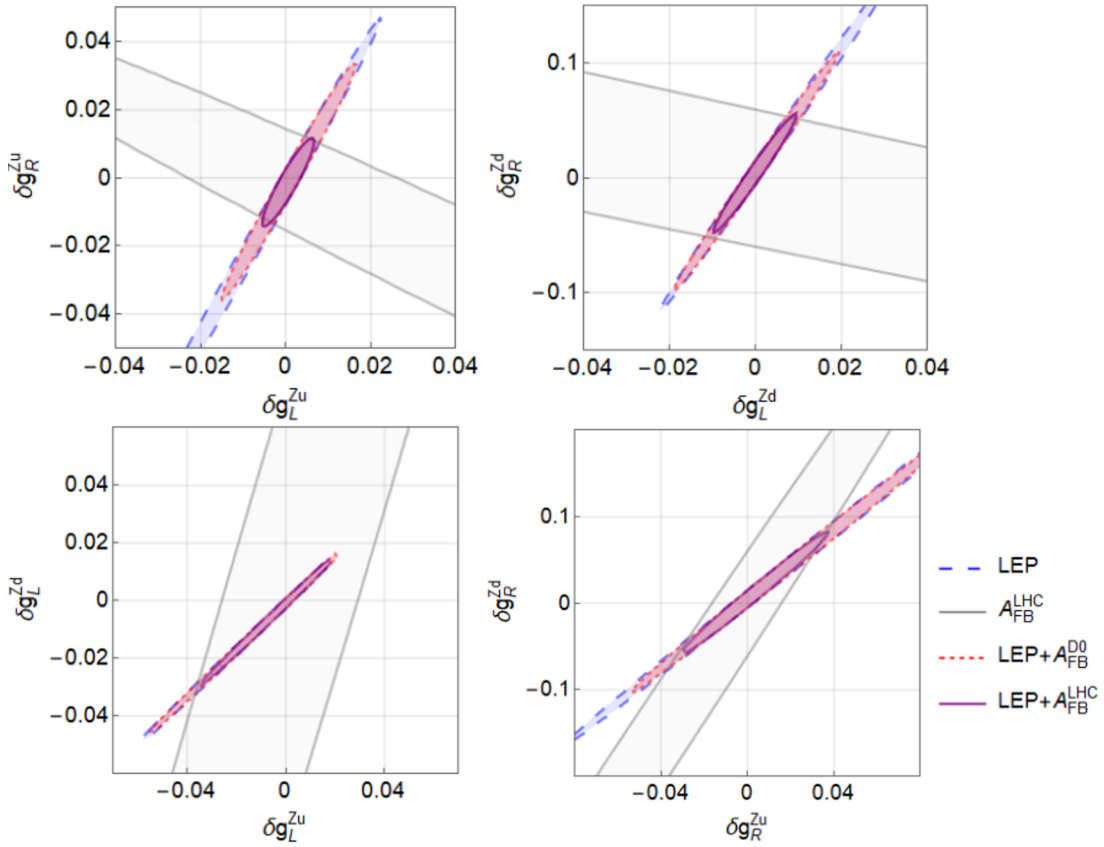

Figure 4. Allowed regions (at 95% CL) for four pairs of corrections of the Z couplings to light quarks. In each case, only that pair of corrections is different from zero, the rest are given by their SM values. Note the scale is different in each panel.

stringent in the D0+LEP case, but the latter are higher in the LHC+LEP case, which reflects the fact that the LHC constrains a specific combination much strongly than D0. This means that both LHC and D0 measurements of the $A_{\rm FB}$ asymmetries bring relevant information to the global fit, although for simple scenarios the LHC will typically have a more important effect, as shown in figure 1, figure 2 (right panel) and figure 4.

However, several caveats should be made concerning the D0 extractions. First, the limits will slightly weaken if one only uses the $A_{\rm FB}$ measurement at the Z pole. Since D0 does not study the dependence of the FB asymmetry with the dilepton rapidity, there is only one measurement at the Z pole. Thus, one will be able to probe only one combination of couplings, contrary to the ATLAS case. Additionally, LHC collaborations are still active and taking data, so one can expect significant improvements on that front.

4.5 Combined fit results

We close this section with a combined fit that includes "traditional" pole observables presented in section 3 (mainly LEP) as well as the above-discussed measurements of the FB asymmetries by ATLAS and D0. The values obtained for the (x, y, z, t) variables are the

JHEP08(2021)021

following:

$$\begin{pmatrix} x \\ y \\ z \\ t \end{pmatrix} = \begin{pmatrix} -0.005 \pm 0.016 \\ 0.009 \pm 0.022 \\ -0.014 \pm 0.032 \\ -0.03 \pm 0.13 \end{pmatrix}, \quad \rho = \begin{pmatrix} 1. & -0.25 & 0.1 & 0.01 \\ -0.25 & 1. & -0.03 & -0.91 \\ 0.1 & -0.03 & 1. & -0.26 \\ 0.01 & -0.91 & -0.26 & 1. \end{pmatrix}, \tag{4.14}$$

Using eq. (3.9) we translate this into constraints on the corrections of the Z couplings to light quarks, which after all are the main subject of our study:

$$\begin{pmatrix} \delta g_L^{Zu} \\ \delta g_R^{Zu} \\ \delta g_L^{Zd} \\ \delta g_R^{Zd} \end{pmatrix} = \begin{pmatrix} -0.012 \pm 0.024 \\ -0.005 \pm 0.032 \\ -0.020 \pm 0.037 \\ -0.03 \pm 0.13 \end{pmatrix}, \quad \rho = \begin{pmatrix} 1 & 0.51 & 0.68 & 0.69 \\ 0.51 & 1 & 0.56 & 0.94 \\ 0.68 & 0.56 & 1 & 0.54 \\ 0.69 & 0.94 & 0.54 & 1 \end{pmatrix}. \tag{4.15}$$

These values are marginalized over the 16 remaining EFT parameters that also contribute to the fit observables, cf. eq. (2.6). The full set of constraints and the $20x20$ correlation matrix is given in appendix B.

5 Conclusions and discussion

In this work we have discussed the impact of LHC Z-pole measurements on constraining the Wilson coefficients of dimension-6 operators in the SMEFT (mainly vertex corrections). Naively, in this domain the LHC should not be able to compete with LEP because the latter measured multiple Z-pole observables with per mille precision in a cleaner environment. However, LEP leaves one unconstrained direction among Z boson couplings to up and down quarks. Indeed, one of the linear combinations defined in eq. (3.9) and denoted as t is not probed at all by LEP observables and represents a flat direction in the $\mathcal{O}(\Lambda^{-2})$ electroweak fit. Information from hadron colliders allows one to plug this hole. In particular, the Drell-Yan $pp \to \ell^+\ell^-$ and $p\bar{p} \to \ell^+\ell^-$ processes are sensitive to the Z boson coupling to light quarks making up the proton and anti-proton. Most importantly for our sake, they are sensitive to a *different* linear combination of these couplings. Therefore, Drell-Yan measurements in hadron colliders are complementary to the LEP observables and provide precious inputs to the electroweak fit. In this paper we exemplified this general fact using the FB asymmetry in $pp \to Z/\gamma^* \to \ell^+\ell^-$ measured by the ATLAS experiment. One of our main results is that the flat direction along the t variable is indeed lifted with the inclusion of the ATLAS input, cf. eq. (4.12). Interestingly enough, we find that the ATLAS $A_{\rm FB}$ information provides a significant improvement on LEP-only bounds on the Zqq vertex corrections even in simple scenarios with few free parameters, as shown in figure 1.

We would like to remark that the importance of hadron colliders for the electroweak fit is more general and goes beyond improving our knowledge of the Zuu and Zdd couplings. This is illustrated in figure 5, where we compare constraints on selected parameters with and without the use of hadron collider observables. First, as shown in this work, constraints on other combinations of $Zq\bar{q}$ couplings, which are denoted as x, y, z and which are probed by LEP, are significantly improved by including information from FB asymmetry in lepton

JHEP08(2021)021

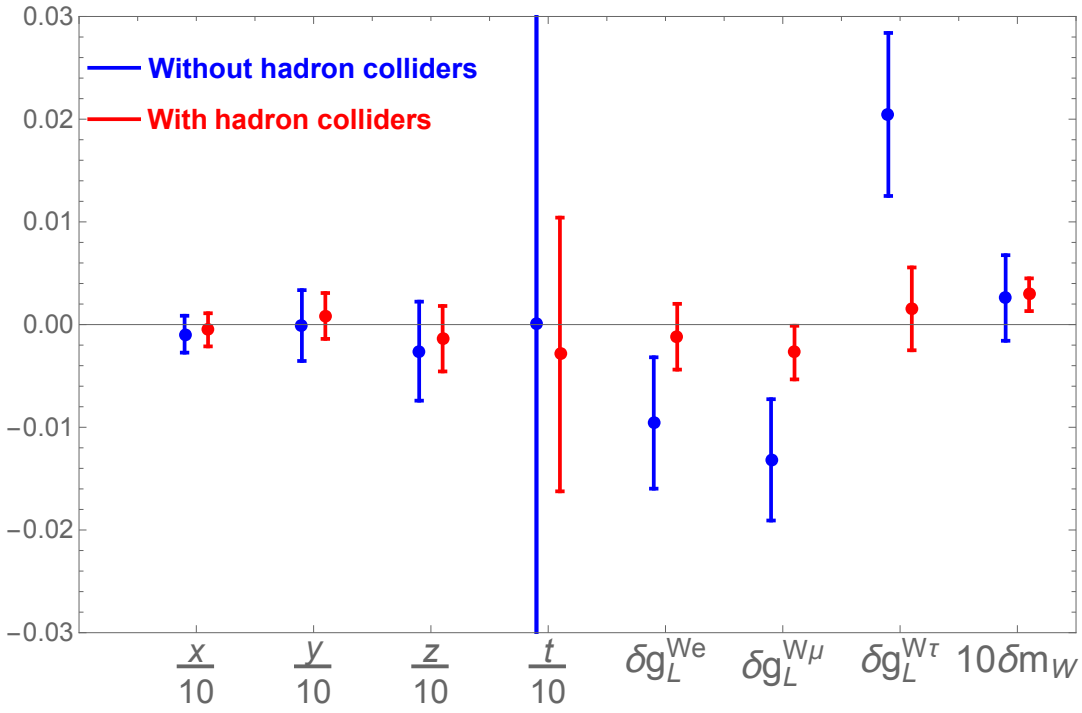

Figure 5. Comparison of the marginalized constraints on selected parameters in the electroweak fit, with (red error bars) and without (blue error bars) using hadron collider observables. Here, x, y, z, t defined in eq. (3.9) are linear combinations of the non-SM corrections to the coupling between the Z boson and light quarks, $\delta g_L^{W\ell}$ are corrections to the coupling between the W boson and left-handed leptons, and δm_W is a correction to the W boson mass.

Drell-Yan production. Even more spectacular improvements happen in the W boson sector. Indeed, LEP could produce $W^\pm$ only in the LEP-2 phase and in much lower numbers than Z, resulting in a lower accuracy of the W observables. It is well known the precision with which the W mass was measured at LEP-2 has been surpassed by the Tevatron and the LHC, which manage to squeeze down the error bar by almost a factor of three. It may be less known that a similar improvement has been achieved for the W boson couplings to leptons. Thanks mainly to the recent measurements of leptonic branching fractions of W in ATLAS and LHCb [12–14] the error bars on the parameters $\delta g_L^{W\ell}$ are improved by approximately a factor of two for $\ell = e, \mu, \tau$. Moreover, tensions with the SM visible in the LEP measurements, which in the past were subject to some theoretical scrutiny [53–55], are now all gone away.

We close with a comment on the perspectives of improving the electroweak fit using future results. Currently, the error for the ATLAS A_4 measurement (used in our study) is dominated by statistics, therefore the bounds on Zqq couplings should be tightened once more data is analyzed. The current and future measurements of Drell-Yan dilepton production by CMS and LHCb could be analyzed following a similar procedure to ours. It is worth noting that Drell-Yan production at the Tevatron, which was a $p\bar{p}$ collider, probes a different combination of the Zqq vertex correction, therefore it would be advantageous to

JHEP08(2021)021

include the final $10\,\text{fb}^{-1}$ Tevatron results in the fit as well. Ideally, all these analyses would be done by the experimental collaboration themselves, who are in the best position to assess the pertinent systematic errors and correlations. Next, information from Drell-Yan cross sections (in addition to asymmetries) could be added, and the off-pole data could be analyzed at the same time in the context of a more general fit to both vertex corrections and 4-fermion operators [56, 57]. Our constraints do not include vertex corrections to the Ztt coupling, but these can be accommodated too in a more comprehensive fit [58–61]. Finally, it would be interesting to analyze the potential of the High-Luminosity LHC [62] and other future colliders for improving the constraints on Zqq vertex corrections. We expect that these future studies will increase even further the impact of hadron colliders on the electroweak precision program.

Acknowledgments

We thank José D. Ruiz-Álvarez for his collaboration in the early stages of this work. VB is supported by Ministerio de Ciencia, Innovación y Universidades, Spain [grant FPU18/01340]. AF has received funding from the Agence Nationale de la Recherche (ANR) under grant ANR-19-CE31-0012 (project MORA) and from the European Union's Horizon 2020 research and innovation programme under the Marie Skłodowska-Curie grant agreement No 860881-HIDDeN. MGA is supported by the *Generalitat Valenciana* (Spain) through the *plan GenT* program (CIDEGENT/2018/014).

A Map to the Warsaw basis

The results of this paper were presented as constraints on the subset of independent vertex corrections defined by the Lagrangian in eq. (2.2). The vertex corrections can be expressed as linear combinations of the Wilson coefficients in any basis of the SMEFT. In this appendix we write down the map to the Warsaw basis.[6] Adopting the conventions and notation of *Wilson coefficient exchange format* (WCxf) [63], the relationship between the independent vertex corrections and the Warsaw basis Wilson coefficients is given by

$$\begin{aligned}
v^{-2}\delta g_L^{We} &= C_{\varphi l}^{(3)} + f(1/2,0) - f(-1/2,-1),\\
v^{-2}\delta g_L^{Ze} &= -\frac{1}{2}C_{\varphi l}^{(3)} - \frac{1}{2}C_{\varphi l}^{(1)} + f(-1/2,-1),\\
v^{-2}\delta g_R^{Ze} &= -\frac{1}{2}C_{\varphi e}^{(1)} + f(0,-1),\\
v^{-2}\delta g_L^{Zu} &= \frac{1}{2}VC_{\varphi q}^{(3)}V^\dagger - \frac{1}{2}VC_{\varphi q}^{(1)}V^\dagger + f(1/2,2/3),\\
v^{-2}\delta g_L^{Zd} &= -\frac{1}{2}C_{\varphi q}^{(3)} - \frac{1}{2}C_{\varphi q}^{(1)} + f(-1/2,-1/3),\\
v^{-2}\delta g_R^{Zu} &= -\frac{1}{2}C_{\varphi u} + f(0,2/3),\\
v^{-2}\delta g_R^{Zd} &= -\frac{1}{2}C_{\varphi d} + f(0,-1/3),
\end{aligned} \tag{A.1}$$

[6] For the map to the SILH basis [26] see ref. [29].

JHEP08(2021)021

where

$$f(T^3,Q)\equiv\left\{-Q\frac{g_Lg_Y}{g_L^2-g_Y^2}C_{\varphi WB}-\left(\frac{1}{4}C_{\varphi D}+\frac{1}{2}\Delta_{G_F}\right)\left(T^3+Q\frac{g_Y^2}{g_L^2-g_Y^2}\right)\right\}\mathbf{1}, \tag{A.2}$$

and $\Delta_{G_F}\equiv[C_{\varphi l}^{(3)}]_{11}+[C_{\varphi l}^{(3)}]_{22}-\frac{1}{2}[C_{ll}]_{1221}$. Moreover, $\delta m_w=\frac{1}{2}[\delta g_L^{We}]_{11}+\frac{1}{2}[\delta g_L^{We}]_{22}-\frac{v^2}{4}[C_{ll}]_{1221}$.

B Complete results and correlation matrix

The marginalized constraints on all 20 independent parameters in our final fit, which uses traditional pole observables (table 1 and table 2), LHC $A_{\rm FB}$ data (table 3) and D0 $A_{\rm FB}$ data [41], are the following:

$$\begin{pmatrix}\delta g_L^{We}\\ \delta g_L^{W\mu}\\ \delta g_L^{W\tau}\\ \delta g_L^{Ze}\\ \delta g_L^{Z\mu}\\ \delta g_L^{Z\tau}\\ \delta g_R^{Ze}\\ \delta g_R^{Z\mu}\\ \delta g_R^{Z\tau}\\ \delta g_L^{Zu}\\ \delta g_R^{Zu}\\ \delta g_L^{Zd}\\ \delta g_R^{Zd}\\ \delta g_L^{Zs}\\ \delta g_R^{Zs}\\ \delta g_L^{Zc}\\ \delta g_R^{Zc}\\ \delta g_L^{Zb}\\ \delta g_R^{Zb}\\ \delta m_w\end{pmatrix}=\begin{pmatrix}-1.2\pm3.2\\ -2.7\pm2.6\\ 1.5\pm4.0\\ -0.20\pm0.28\\ 0.1\pm1.2\\ -0.09\pm0.59\\ -0.43\pm0.27\\ 0.0\pm1.4\\ 0.62\pm0.62\\ -12\pm24\\ -5\pm32\\ -20\pm37\\ -30\pm130\\ 11\pm28\\ 32\pm48\\ -1.5\pm3.6\\ -3.3\pm5.3\\ 3.1\pm1.7\\ 21.9\pm8.8\\ 0.29\pm0.16\end{pmatrix}\times10^{-3}. \tag{B.1}$$

JHEP08(2021)021

The correlation matrix is

$$\begin{pmatrix}
1 & 0.2 & -0.59 & -0.22 & -0.09 & 0.01 & 0.16 & -0.13 & -0.08 & -0.04 & -0.06 & -0.03 & -0.06 & -0.02 & -0.04 & -0.01 & 0.01 & 0.04 & 0.01 & 0. \\
- & 1 & -0.39 & -0.27 & -0.11 & 0.01 & 0.2 & -0.16 & -0.1 & -0.04 & -0.06 & -0.03 & -0.07 & -0.03 & -0.04 & -0.01 & 0.01 & 0.05 & 0.01 & 0. \\
- & - & 1 & -0.18 & -0.07 & 0.01 & 0.13 & -0.11 & -0.07 & 0. & 0. & 0. & 0. & 0. & 0. & -0.01 & 0. & 0.04 & 0.01 & 0. \\
- & - & - & 1 & -0.09 & -0.07 & 0.16 & -0.04 & 0.04 & 0.04 & 0.06 & 0.03 & 0.06 & 0.03 & 0.04 & 0.07 & 0.08 & -0.36 & -0.35 & 0. \\
- & - & - & - & 1 & 0.06 & -0.04 & 0.91 & -0.04 & 0. & 0.01 & 0.01 & 0.01 & 0.01 & 0.01 & -0.02 & -0.01 & 0.06 & 0.04 & 0. \\
- & - & - & - & - & 1 & 0.02 & -0.03 & 0.41 & -0.01 & -0.01 & -0.01 & -0.02 & 0. & -0.01 & -0.02 & 0.01 & 0.07 & 0.01 & 0. \\
- & - & - & - & - & - & 1 & -0.07 & -0.04 & -0.02 & -0.03 & -0.02 & -0.03 & -0.01 & -0.02 & 0.06 & 0.11 & -0.34 & -0.38 & 0. \\
- & - & - & - & - & - & - & 1 & 0.04 & 0.02 & 0.03 & 0.02 & 0.03 & 0.01 & 0.02 & 0. & -0.01 & 0.01 & 0.03 & 0. \\
- & - & - & - & - & - & - & - & 1 & 0.02 & 0.03 & 0.01 & 0.03 & 0.01 & 0.02 & 0.01 & -0.01 & -0.04 & 0. & 0. \\
- & - & - & - & - & - & - & - & - & 1 & 0.5 & 0.68 & 0.69 & 0.07 & -0.29 & -0.05 & 0.09 & -0.02 & -0.01 & 0. \\
- & - & - & - & - & - & - & - & - & - & 1 & 0.55 & 0.94 & -0.11 & -0.39 & 0.07 & 0.07 & -0.03 & -0.02 & 0. \\
- & - & - & - & - & - & - & - & - & - & - & 1 & 0.54 & -0.64 & -0.08 & -0.02 & 0.05 & -0.01 & 0. & 0. \\
- & - & - & - & - & - & - & - & - & - & - & - & 1 & 0.07 & -0.46 & 0.05 & 0.09 & -0.03 & -0.02 & 0. \\
- & - & - & - & - & - & - & - & - & - & - & - & - & 1 & -0.01 & 0.1 & 0.03 & -0.02 & -0.01 & 0. \\
- & - & - & - & - & - & - & - & - & - & - & - & - & - & 1 & 0.04 & 0.05 & -0.02 & -0.01 & 0. \\
- & - & - & - & - & - & - & - & - & - & - & - & - & - & - & 1 & 0.32 & -0.11 & -0.15 & 0. \\
- & - & - & - & - & - & - & - & - & - & - & - & - & - & - & - & 1 & -0.17 & -0.14 & 0. \\
- & - & - & - & - & - & - & - & - & - & - & - & - & - & - & - & - & 1 & 0.9 & 0. \\
- & - & - & - & - & - & - & - & - & - & - & - & - & - & - & - & - & - & 1 & 0. \\
- & - & - & - & - & - & - & - & - & - & - & - & - & - & - & - & - & - & - & 1
\end{pmatrix}.$$

Despite appearances, the W mass corrections δm_w is not completely uncorrelated with the vertex correction, but the correlation coefficients are of order 0.001, and are approximated as zero above.

The results above are enough to reproduce the full Gaussian likelihood function for our parameters.[7] Using the map in eq. (A.1), it can be translated into a likelihood for the Wilson coefficients in the Warsaw basis at the scale $\mu = m_Z$. In this step, the map should be used for $V \to \mathbf{I}$, since our fit results are formally valid in this limit. That can be evolved to other RG scales using e.g. the public code `DsixTools` [64] or `Wilson` [65]. Our general likelihood can always be restricted to more constrained flavor scenarios [66, 67] or to the universal scenario with oblique parameters [68]. We close this appendix with the limits that we find when considering one operator at a time in figure 6 and figure 7.

[7] This likelihood function is also available on request as a `Mathematica` notebook.

JHEP08(2021)021

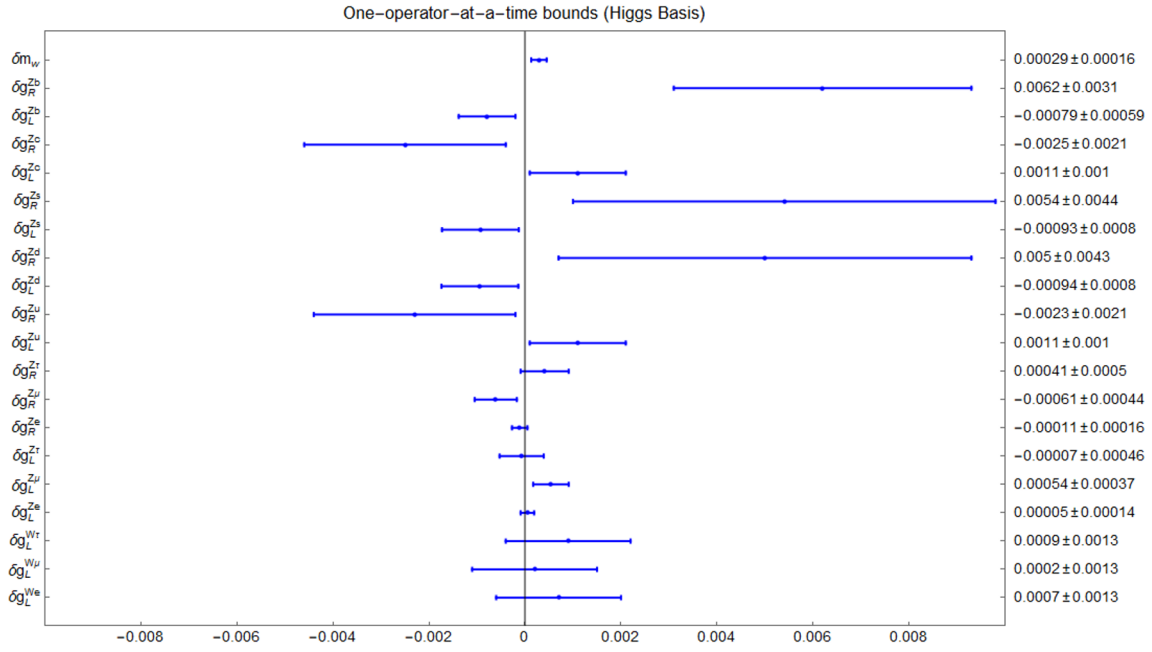

Figure 6. Constraints obtained from our final electroweak fit, which uses traditional pole observables (table 1 and table 2), LHC $A_{\rm FB}$ data (table 3) and D0 $A_{\rm FB}$ data [41], when considering one Higgs-basis operator at a time.

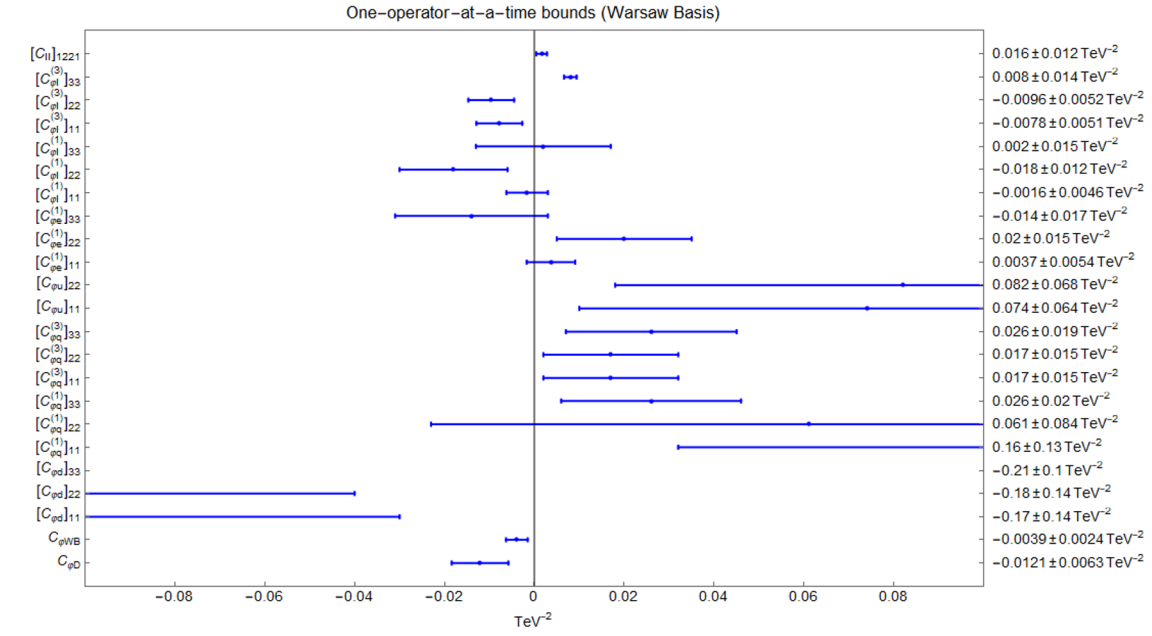

Figure 7. Constraints obtained from our final electroweak fit, which uses traditional pole observables (table 1 and table 2), LHC $A_{\rm FB}$ data (table 3) and D0 $A_{\rm FB}$ data [41], when considering one Warsaw-basis operator at a time.

JHEP08(2021)021

References

[1] C.N. Leung, S.T. Love and S. Rao, *Low-Energy Manifestations of a New Interaction Scale: Operator Analysis*, *Z. Phys. C* **31** (1986) 433 [INSPIRE].

[2] W. Buchmüller and D. Wyler, *Effective Lagrangian Analysis of New Interactions and Flavor Conservation*, *Nucl. Phys. B* **268** (1986) 621 [INSPIRE].

[3] J. de Blas, J.C. Criado, M. Pérez-Victoria and J. Santiago, *Effective description of general extensions of the Standard Model: the complete tree-level dictionary*, *JHEP* **03** (2018) 109 [arXiv:1711.10391] [INSPIRE].

[4] ALEPH, DELPHI, L3, OPAL, SLD, LEP Electroweak Working Group, SLD Electroweak Group and SLD Heavy Flavour Group collaborations, *Precision electroweak measurements on the Z resonance*, *Phys. Rept.* **427** (2006) 257 [hep-ex/0509008] [INSPIRE].

[5] ALEPH, DELPHI, L3, OPAL and LEP Electroweak collaborations, *Electroweak Measurements in Electron-Positron Collisions at W-Boson-Pair Energies at LEP*, *Phys. Rept.* **532** (2013) 119 [arXiv:1302.3415] [INSPIRE].

[6] M.E. Peskin and T. Takeuchi, *Estimation of oblique electroweak corrections*, *Phys. Rev. D* **46** (1992) 381 [INSPIRE].

[7] Z. Han and W. Skiba, *Effective theory analysis of precision electroweak data*, *Phys. Rev. D* **71** (2005) 075009 [hep-ph/0412166] [INSPIRE].

[8] ATLAS collaboration, *Measurement of the W-boson mass in pp collisions at $\sqrt{s} = 7$ TeV with the ATLAS detector*, *Eur. Phys. J. C* **78** (2018) 110 [*Erratum ibid.* **78** (2018) 898] [arXiv:1701.07240] [INSPIRE].

[9] Particle Data Group collaboration, *Review of Particle Physics*, *PTEP* **2020** (2020) 083C01 [INSPIRE].

[10] CDF collaboration, *A Direct measurement of the W boson width in $p\bar{p}$ collisions at $\sqrt{s} = 1.96-$TeV*, *Phys. Rev. Lett.* **100** (2008) 071801 [arXiv:0710.4112] [INSPIRE].

[11] D0 collaboration, *Direct measurement of the W boson width*, *Phys. Rev. Lett.* **103** (2009) 231802 [arXiv:0909.4814] [INSPIRE].

[12] LHCb collaboration, *Measurement of forward $W \to e\nu$ production in pp collisions at $\sqrt{s} = 8$ TeV*, *JHEP* **10** (2016) 030 [arXiv:1608.01484] [INSPIRE].

[13] ATLAS collaboration, *Precision measurement and interpretation of inclusive W^+, W^- and Z/γ^* production cross sections with the ATLAS detector*, *Eur. Phys. J. C* **77** (2017) 367 [arXiv:1612.03016] [INSPIRE].

[14] ATLAS collaboration, *Test of the universality of τ and μ lepton couplings in W-boson decays from $t\bar{t}$ events with the ATLAS detector*, arXiv:2007.14040 [INSPIRE].

[15] LHCb collaboration, *Measurement of the forward-backward asymmetry in $Z/\gamma^* \to \mu^+\mu^-$ decays and determination of the effective weak mixing angle*, *JHEP* **11** (2015) 190 [arXiv:1509.07645] [INSPIRE].

JHEP08(2021)021

[16] ATLAS collaboration, *Measurement of the forward-backward asymmetry of electron and muon pair-production in pp collisions at $\sqrt{s} = 7$ TeV with the ATLAS detector*, *JHEP* **09** (2015) 049 [arXiv:1503.03709] [INSPIRE].

[17] CMS collaboration, *Measurement of the weak mixing angle using the forward-backward asymmetry of Drell-Yan events in pp collisions at 8 TeV*, *Eur. Phys. J. C* **78** (2018) 701 [arXiv:1806.00863] [INSPIRE].

[18] CMS collaboration, *Forward-backward asymmetry of Drell-Yan lepton pairs in pp collisions at $\sqrt{s} = 8$ TeV*, *Eur. Phys. J. C* **76** (2016) 325 [arXiv:1601.04768] [INSPIRE].

[19] ATLAS collaboration, *Measurement of the Drell-Yan triple-differential cross section in pp collisions at $\sqrt{s} = 8$ TeV*, *JHEP* **12** (2017) 059 [arXiv:1710.05167] [INSPIRE].

[20] V. Cirigliano, M. Gonzalez-Alonso and M.L. Graesser, *Non-standard Charged Current Interactions: beta decays versus the LHC*, *JHEP* **02** (2013) 046 [arXiv:1210.4553] [INSPIRE].

[21] J. de Blas, M. Chala and J. Santiago, *Global Constraints on Lepton-Quark Contact Interactions*, *Phys. Rev. D* **88** (2013) 095011 [arXiv:1307.5068] [INSPIRE].

[22] A. Greljo and D. Marzocca, *High-p_T dilepton tails and flavor physics*, *Eur. Phys. J. C* **77** (2017) 548 [arXiv:1704.09015] [INSPIRE].

[23] P. Fisher, U. Becker and J. Kirkby, *Very high precision tests of the electroweak theory*, *Phys. Lett. B* **356** (1995) 404 [INSPIRE].

[24] M. Dittmar, *Neutral current interference in the TeV region: The Experimental sensitivity at the LHC*, *Phys. Rev. D* **55** (1997) 161 [hep-ex/9606002] [INSPIRE].

[25] B. Grzadkowski, M. Iskrzynski, M. Misiak and J. Rosiek, *Dimension-Six Terms in the Standard Model Lagrangian*, *JHEP* **10** (2010) 085 [arXiv:1008.4884] [INSPIRE].

[26] R. Contino, M. Ghezzi, C. Grojean, M. Muhlleitner and M. Spira, *Effective Lagrangian for a light Higgs-like scalar*, *JHEP* **07** (2013) 035 [arXiv:1303.3876] [INSPIRE].

[27] S. Descotes-Genon, A. Falkowski, M. Fedele, M. González-Alonso and J. Virto, *The CKM parameters in the SMEFT*, *JHEP* **05** (2019) 172 [arXiv:1812.08163] [INSPIRE].

[28] S. Dawson and P.P. Giardino, *Electroweak and QCD corrections to Z and W pole observables in the standard model EFT*, *Phys. Rev. D* **101** (2020) 013001 [arXiv:1909.02000] [INSPIRE].

[29] LHC Higgs Cross Section Working Group collaboration, *Handbook of LHC Higgs Cross Sections: 4. Deciphering the Nature of the Higgs Sector*, arXiv:1610.07922 [INSPIRE].

[30] P. Janot and S. Jadach, *Improved Bhabha cross section at LEP and the number of light neutrino species*, *Phys. Lett. B* **803** (2020) 135319 [arXiv:1912.02067] [INSPIRE].

[31] D. d'Enterria and C. Yan, *Revised QCD effects on the $Z \to b\bar{b}$ forward-backward asymmetry*, arXiv:2011.00530 [INSPIRE].

[32] SLD collaboration, *First direct measurement of the parity violating coupling of the Z0 to the s quark*, *Phys. Rev. Lett.* **85** (2000) 5059 [hep-ex/0006019] [INSPIRE].

[33] D0 collaboration, *A measurement of the $W \to \tau\nu$ production cross section in $p\bar{p}$ collisions at $\sqrt{s} = 1.8$ TeV*, *Phys. Rev. Lett.* **84** (2000) 5710 [hep-ex/9912065] [INSPIRE].

[34] CDF collaboration, *Measurements of inclusive W and Z cross sections in $p\bar{p}$ collisions at $\sqrt{s} = 1.96$ TeV*, *J. Phys. G* **34** (2007) 2457 [hep-ex/0508029] [INSPIRE].

JHEP08(2021)021

[35] A. Falkowski and D. Straub, *Flavourful SMEFT likelihood for Higgs and electroweak data*, *JHEP* **04** (2020) 066 [arXiv:1911.07866] [INSPIRE].

[36] D. d'Enterria and V. Jacobsen, *Improved strong coupling determinations from hadronic decays of electroweak bosons at N^3LO accuracy*, arXiv:2005.04545 [INSPIRE].

[37] M. Awramik, M. Czakon, A. Freitas and G. Weiglein, *Precise prediction for the W boson mass in the standard model*, *Phys. Rev. D* **69** (2004) 053006 [hep-ph/0311148] [INSPIRE].

[38] R. Alonso, E.E. Jenkins, A.V. Manohar and M. Trott, *Renormalization Group Evolution of the Standard Model Dimension Six Operators III: Gauge Coupling Dependence and Phenomenology*, *JHEP* **04** (2014) 159 [arXiv:1312.2014] [INSPIRE].

[39] S. Dawson, S. Homiller and S.D. Lane, *Putting standard model EFT fits to work*, *Phys. Rev. D* **102** (2020) 055012 [arXiv:2007.01296] [INSPIRE].

[40] A. Efrati, A. Falkowski and Y. Soreq, *Electroweak constraints on flavorful effective theories*, *JHEP* **07** (2015) 018 [arXiv:1503.07872] [INSPIRE].

[41] D0 collaboration, *Measurement of $\sin^2\theta^\ell_{\rm eff}$ and Z-light quark couplings using the forward-backward charge asymmetry in $p\bar{p} \to Z/\gamma^* \to e^+e^-$ events with $\mathcal{L} = 5.0\,fb^{-1}$ at $\sqrt{s} = 1.96\,TeV$*, *Phys. Rev. D* **84** (2011) 012007 [arXiv:1104.4590] [INSPIRE].

[42] E. Accomando, J. Fiaschi, F. Hautmann and S. Moretti, *Neutral current forward-backward asymmetry: from θ_W to PDF determinations*, *Eur. Phys. J. C* **78** (2018) 663 [*Erratum ibid.* **79** (2019) 453] [arXiv:1805.09239] [INSPIRE].

[43] A. Bodek, J. Han, A. Khukhunaishvili and W. Sakumoto, *Using Drell-Yan forward-backward asymmetry to reduce PDF uncertainties in the measurement of electroweak parameters*, *Eur. Phys. J. C* **76** (2016) 115 [arXiv:1507.02470] [INSPIRE].

[44] CMS collaboration, *Measurement of the weak mixing angle with the Drell-Yan process in proton-proton collisions at the LHC*, *Phys. Rev. D* **84** (2011) 112002 [arXiv:1110.2682] [INSPIRE].

[45] J.C. Collins and D.E. Soper, *Angular Distribution of Dileptons in High-Energy Hadron Collisions*, *Phys. Rev. D* **16** (1977) 2219 [INSPIRE].

[46] ATLAS collaboration, *Measurement of the effective leptonic weak mixing angle using electron and muon pairs from Z-boson decay in the ATLAS experiment at $\sqrt{s} = 8\,TeV$*, CERN, Geneva (2018) ATLAS-CONF-2018-037.

[47] G. Bozzi, S. Catani, G. Ferrera, D. de Florian and M. Grazzini, *Production of Drell-Yan lepton pairs in hadron collisions: Transverse-momentum resummation at next-to-next-to-leading logarithmic accuracy*, *Phys. Lett. B* **696** (2011) 207 [arXiv:1007.2351] [INSPIRE].

[48] S. Catani, D. de Florian, G. Ferrera and M. Grazzini, *Vector boson production at hadron colliders: transverse-momentum resummation and leptonic decay*, *JHEP* **12** (2015) 047 [arXiv:1507.06937] [INSPIRE].

[49] S. Catani, L. Cieri, G. Ferrera, D. de Florian and M. Grazzini, *Vector boson production at hadron colliders: a fully exclusive QCD calculation at NNLO*, *Phys. Rev. Lett.* **103** (2009) 082001 [arXiv:0903.2120] [INSPIRE].

[50] L.A. Harland-Lang, A.D. Martin, P. Motylinski and R.S. Thorne, *Parton distributions in the LHC era: MMHT 2014 PDFs*, *Eur. Phys. J. C* **75** (2015) 204 [arXiv:1412.3989] [INSPIRE].

JHEP08(2021)021

[51] J. Alwall et al., *The automated computation of tree-level and next-to-leading order differential cross sections, and their matching to parton shower simulations*, *JHEP* **07** (2014) 079 [arXiv:1405.0301] [INSPIRE].

[52] E. Conte, B. Fuks and G. Serret, *MadAnalysis 5, A User-Friendly Framework for Collider Phenomenology*, *Comput. Phys. Commun.* **184** (2013) 222 [arXiv:1206.1599] [INSPIRE].

[53] R. Dermisek, *Light Charged Higgs and Lepton Universality in W boson Decays*, arXiv:0807.2135 [INSPIRE].

[54] A. Filipuzzi, J. Portoles and M. Gonzalez-Alonso, $U(2)^5$ *flavor symmetry and lepton universality violation in* $W \to \tau\nu_\tau$, *Phys. Rev. D* **85** (2012) 116010 [arXiv:1203.2092] [INSPIRE].

[55] W. Mader, J.-h. Park, G.M. Pruna, D. Stöckinger and A. Straessner, *LHC Explores What LEP Hinted at: CP-Violating Type-I 2HDM*, *JHEP* **09** (2012) 125 [*Erratum ibid.* **01** (2014) 006] [arXiv:1205.2692] [INSPIRE].

[56] A. Falkowski, M. González-Alonso and K. Mimouni, *Compilation of low-energy constraints on 4-fermion operators in the SMEFT*, *JHEP* **08** (2017) 123 [arXiv:1706.03783] [INSPIRE].

[57] A. Horne, J. Pittman, M. Snedeker, W. Shepherd and J.W. Walker, *Shift-Type SMEFT Effects in Dileptons at the LHC*, *JHEP* **03** (2021) 118 [arXiv:2007.12698] [INSPIRE].

[58] A. Buckley et al., *Global fit of top quark effective theory to data*, *Phys. Rev. D* **92** (2015) 091501 [arXiv:1506.08845] [INSPIRE].

[59] D. Barducci et al., *Interpreting top-quark LHC measurements in the standard-model effective field theory*, arXiv:1802.07237 [INSPIRE].

[60] J. Ellis, M. Madigan, K. Mimasu, V. Sanz and T. You, *Top, Higgs, Diboson and Electroweak Fit to the Standard Model Effective Field Theory*, *JHEP* **04** (2021) 279 [arXiv:2012.02779] [INSPIRE].

[61] S. Bruggisser, R. Schäfer, D. van Dyk and S. Westhoff, *The Flavor of UV Physics*, *JHEP* **05** (2021) 257 [arXiv:2101.07273] [INSPIRE].

[62] ATLAS collaboration, *Prospect for a measurement of the Weak Mixing Angle in* $pp \to Z/\gamma^* \to e^+e^-$ *events with the ATLAS detector at the High Luminosity Large Hadron Collider*, Tech. Rep. ATL-PHYS-PUB-2018-037, CERN, Geneva (Nov, 2018).

[63] J. Aebischer et al., *WCxf: an exchange format for Wilson coefficients beyond the Standard Model*, *Comput. Phys. Commun.* **232** (2018) 71 [arXiv:1712.05298] [INSPIRE].

[64] A. Celis, J. Fuentes-Martin, A. Vicente and J. Virto, *DsixTools: The Standard Model Effective Field Theory Toolkit*, *Eur. Phys. J. C* **77** (2017) 405 [arXiv:1704.04504] [INSPIRE].

[65] J. Aebischer, J. Kumar and D.M. Straub, *Wilson: a Python package for the running and matching of Wilson coefficients above and below the electroweak scale*, *Eur. Phys. J. C* **78** (2018) 1026 [arXiv:1804.05033] [INSPIRE].

[66] R. Aoude, T. Hurth, S. Renner and W. Shepherd, *The impact of flavour data on global fits of the MFV SMEFT*, *JHEP* **12** (2020) 113 [arXiv:2003.05432] [INSPIRE].

[67] D.A. Faroughy, G. Isidori, F. Wilsch and K. Yamamoto, *Flavour symmetries in the SMEFT*, *JHEP* **08** (2020) 166 [arXiv:2005.05366] [INSPIRE].

[68] J.D. Wells and Z. Zhang, *Effective theories of universal theories*, *JHEP* **01** (2016) 123 [arXiv:1510.08462] [INSPIRE].

JHEP08(2021)021